PCCP

PAPER

Cite this: *Phys. Chem. Chem. Phys.*, 2017, **19**, 25391

Elastic and viscous bond components in the adhesion of colloidal particles and fibrillated streptococci to QCM-D crystal surfaces with different hydrophobicities using Kelvin–Voigt and Maxwell models

Rebecca van der Westen,[a] Prashant K. Sharma, †*[a] Hans De Raedt,[b] Ijsbrand Vermue,[a] Henny C. van der Mei [a] and Henk J. Busscher [a]

Received 11th July 2017,
Accepted 22nd August 2017

DOI: 10.1039/c7cp04676f

rsc.li/pccp

A quartz-crystal-microbalance with dissipation (QCM-D) can measure molecular mass adsorption as well as register adhesion of colloidal particles. However, analysis of the QCM-D output to quantitatively analyze adhesion of (bio)colloids to obtain viscoelastic bond properties is still a subject of debate. Here, we analyze the QCM-D output to analyze the bond between two hydrophilic streptococcal strains 91 nm long and without fibrillar surface appendages and micron-sized hydrophobic polystyrene particles on QCM-D crystal surfaces with different hydrophobicities, using the Kelvin–Voigt model and the Maxwell model. A Poisson distribution was implemented in order to determine the possible virtues of including polydispersity when fitting model parameters to the data. The quality of the fits did not indicate whether the Kelvin–Voigt or the Maxwell model is preferable and only polydispersity in spring-constants improved the fit for polystyrene particles. The Kelvin–Voigt and Maxwell models both yielded higher spring-constants for the bald streptococcus than for the fibrillated one. In both models, the drag coefficients increased for the bald streptococcus with the ratio of electron-donating over electron-accepting parameters of the crystal surface, while for the fibrillated strain the drag coefficient was similar on all crystal surfaces. Combined with the propensity of fibrillated streptococci to bind to the sensor crystal as a coupled-resonator above the crystal surface, this suggests that the drag experienced by resonator-coupled, hydrophilic particles is more influenced by the viscosity of the bulk water than by interfacial water adjacent to the crystal surface. Hydrophilic particles that lack a surface tether are mass-coupled just above the crystal surface and accordingly probe the drag due to the thin layer of interfacial water that is differently structured on hydrophobic and hydrophilic surfaces. Hydrophobic particles without a surface tether are also mass-coupled, but their drag coefficient decreases when the ratio of electron-donating over electron-accepting parameters increases, suggesting that hydrophobic particles experience less drag due to the structured water adjacent to the surface.

Introduction

The bond between colloidal particles adhering to a substratum surface is often considered rigid,[1] but in reality it consists of an elastic and a viscous component, which is especially the case when working with bio-colloids, like bacteria.[2] Bacteria can bind to surfaces through a variety of different surface appendages such as fibrils and fimbriae of various lengths,[3] adding to the viscoelasticity of the bond. The viscoelastic nature of the bacterium–substratum bond can be described by combinations of a linearly responding[4,5] spring and a dashpot, in which the spring represents the elasticity of the tether and the dashpot represents the viscous drag. The spring and the dashpot can either be placed in parallel (Kelvin–Voigt model, see Fig. 1a) or in series (Maxwell model, see Fig. 1b). The dashpot slows down the response speed, generally referred to as damping.[6] Viscoelasticity of bacterial binding has been described as a means to

[a] *University of Groningen and University Medical Center Groningen, Department of Biomedical Engineering, Antonius Deusinglaan 1, 9713AV, Groningen, The Netherlands*
[b] *Faculty of Mathematics and Natural Sciences, Computational Physics, Zernike Institute for Advanced Materials, Nijenborgh 4, 9747 AG Groningen, The Netherlands*
† Department of Biomedical Engineering, University Medical Center Groningen and University of Groningen, P.O. Box 196, 9700 AD, Groningen, The Netherlands. E-mail: p.k.sharma@umcg.nl; Tel: +31 50 3616097, +31 50 3616094

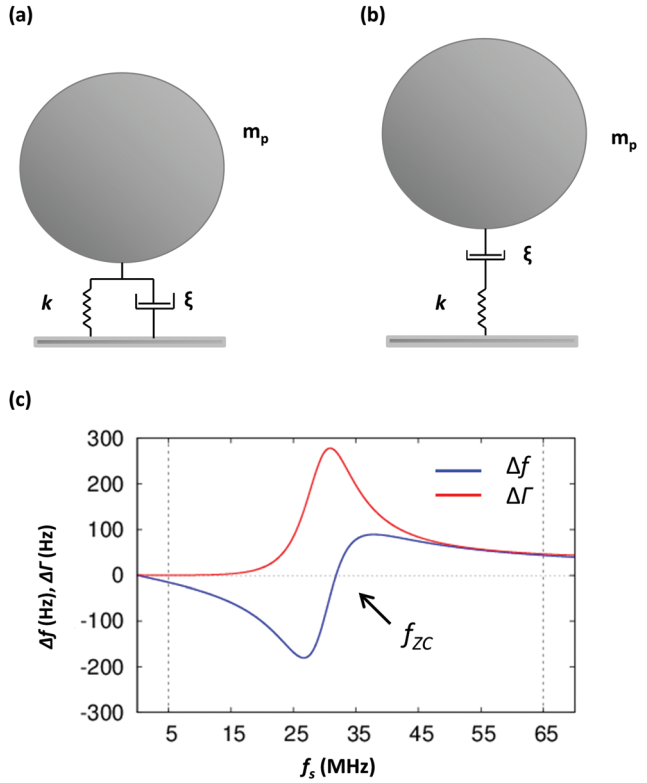

Fig. 1 (a and b) Mechanical equivalent circuit representing a particle with mass, m_p tethered to a surface *via* a viscoelastic bond containing a spring with spring constant (k) and a dashpot with a drag coefficient (ξ) in parallel (a: Kelvin–Voigt model) and in series (b: Maxwell model). (c) Schematic presentation of the shifts in resonance frequency and dissipation in QCM-D as a function of the crystal resonance frequency in a coupled resonator model according to Kelvin–Voigt. The frequency of zero crossing is chosen within the observable window of the sensor resonance frequency and its overtones at which the resonance frequencies of the crystal (f_s) and of the adhering particles (the particle resonance frequency f_p, taken here as 30 Hz) match. Input parameters for the generation of this graph according to eqn (1): f_F = 5 MHz, $m_p = 3 \times 10^{-16}$ kg, $\omega_p = 2\pi \times f_p$ Hz, $\omega_s = 2\pi \times f_s$, where f_s is in the range between 5 and 65 MHz, ($Z_q = 8.8 \times 10^6$ kg m^{-2} s^{-1}), ($N_p = 1.1 \times 10^{10}$ m^{-2}). Note: dissipation is expressed as $\Delta\Gamma$ according to $\Delta\Gamma = \Delta D \times f_s/2$ (see the Data analysis section).

allow bacteria more time to react in an appropriate way to catastrophic events, such as removal forces or chemical attack.[6,7]

The response kinetics of adhering bacteria to an applied stress differs considerably when the dashpot is placed in parallel with the spring (Fig. 1a), damping any spring response, or when both elements are placed in series (Fig. 1b), allowing an immediate spring response followed by a delayed response due to the dashpot.[8] The viscoelastic response of adhering single bacteria under stress has been studied using Atomic Force Microscopy (AFM) and modeled to a one-element Maxwell model.[2,9,10] Bacterial inhabitants in a biofilm adhere to a substratum surface and to each other and their stress response to low load compression[11,12] has been modeled using a series of Maxwell elements in parallel. Analysis of Brownian motion induced nanoscopic vibrations of single bacteria[13] and abiotic particles[14,15] adhering to substratum surfaces can also yield spring constants of binding tethers, but similar to AFM and optical tweezer-analyses[16] yields data that are accompanied by large standard deviations. This suggests a polydispersity of the binding tether characteristics. At the same time, the viscoelastic response of adhering bacteria or abiotic particles obtained employing a Quartz Crystal Microbalance with Dissipation (QCM-D) has been fitted with phenomenological models, such as the Kelvin–Voigt[17] model or the Maxwell model.[5]

The aim of this study is to analyze the QCM-D response to adhesion of a fibrillated and a non-fibrillated streptococcal strain using Kelvin–Voigt or Maxwell coupled resonator models. Abiotic polystyrene particles have been included for comparison, while QCM-D crystal surfaces have been applied possessing different hydrophobicities to determine whether either of the two models would be better applicable for particles adhering on a hydrophobic or hydrophilic surface. In addition, possible advantages of extending either phenomenological model with a polydispersity index are explored.

QCM-D is widely used in molecular adsorption. As per the conventional mass loading theory,[18] the adsorbed mass couples directly to the sensor surface (an AT-cut quartz crystal) increasing its effective mass, reducing its resonance frequency and leading to negative shifts in resonance frequency (Δf). Mass loading is mostly observed when molecular layers adhering to the sensor surface are thinner than 250 nm. The viscoelastic properties of the bond between an adhering mass and a substratum surface in the QCM-D can cause dissipation (ΔD). In contrast to molecular adsorption, colloidal particles adhere to the sensor surface *via* a tethered, non-rigid bond, causing positive frequency shifts, as schematically outlined in Fig. 1c.[19–21] Positive frequency shifts can be explained[19] assuming that the adhering particles and the QCM-D crystal sensor act as coupled resonators.[17,22,23] The maximal energy dissipation change (ΔD) occurs when the particle resonance frequency (f_p) matches the crystal sensor resonance frequency (f_s). Moreover, QCM-D can identify a zero-value in the sensor resonance frequency shift (Δf_s) when the particle and the crystal sensor resonance frequencies match, referred to as the frequency of zero-crossing (f_{ZC}) (see Fig. 1c). Zero crossing frequencies can only be observed when occurring within the range of the sensor crystal resonance frequency and its overtones, usually between 5 and 65 MHz (see also Fig. 1c).

The elastic and viscous contributions to the bond can be evaluated by assuming the bond to be either Kelvin–Voigt or Maxwell in nature (Fig. 1a or Fig. 1b) according to eqn (1)[17] or eqn (2),[5,8] respectively,

$$\Delta f + \frac{i\Delta D f_s}{2} = \frac{f_F m_p}{\pi Z_q} \cdot N_p \left[\frac{\omega_s^3(\omega_p^2 - \gamma^2) - \omega_s \omega_p^4}{(\omega_s^2 - \omega_p^2)^2 + \omega_s^2 \gamma^2} + i \frac{\omega_s^4 \gamma}{(\omega_s^2 - \omega_p^2)^2 + \omega_s^2 \gamma^2} \right] \quad (1)$$

$$\Delta f + \frac{i\Delta D f_s}{2} = \frac{f_F N_p}{\pi Z_q} \cdot \left[i\omega_s m_p \frac{1}{1 - \frac{\omega_s^2}{\omega_p^2} + \frac{i\omega}{\gamma}} \right] \quad (2)$$

where ΔD is the shift in dissipation, f_F is the fundamental frequency of the crystal (5 MHz), m_p is the inertial mass of the particle in kg, ω_p is the resonance angular frequency for the particle, ω_s is the sensor angular frequency, Z_q is the acoustic impedance of an AT-cut quartz crystal (8.8×10^6 kg m^{-2} s^{-1}), and N_p is the number of adhering particles per unit area (m^{-2}). Eqn (1) and (2) can be simply derived using the basic QCM-D equation and inserting the mechanical analogues of a Kelvin–Voigt or Maxwell element. Since the QCM-D is a mechanical system, the rules for adding mechanical impedances differ from the rules for adding impedances in electricity: when mechanical elements operate in parallel, the total impedance is additive, opposite to when they operate in series in which case the inverse total impedance is the sum of the inverse impedance of the individual elements.[24]

γ, ω_p and m_p can be derived from eqn (1) or eqn (2) for both models without accounting for polydispersity, using a brute-force, iterative procedure, as recently described for a Kelvin–Voigt model[25] and that can be analogously applied to a Maxwell model. As $\omega_p = \sqrt{\frac{k}{m_p}}$, the spring constant k can be directly calculated, while since $\gamma = \xi/m_p$ the drag coefficient, ξ immediately follows. Although the inertial mass m_p does not necessarily have to be equal to the gravitational mass of the particles, order of magnitude matching has been suggested for validation of physically realistic results of the brute-force, iterative procedure.[25]

In order to account for a possible polydispersity in inertial mass, spring constant and drag-force (m_p, k and ξ, respectively) as suggested by the large standard deviations in AFM, optical tweezer and vibration analyses of colloidal bond characteristics, a Poisson distribution can be implemented into the above equations according to[26]

$$p(n,x) = \frac{\lambda^n e^{-\lambda}}{n!} \tag{3}$$

where λ indicates both the mean and variance of the distribution where n goes from 0 to N. In order to account for polydispersity, eqn (1) and (2) transform to eqn (4).

$$\begin{aligned}\Delta f + \frac{i\Delta D f_s}{2} = {} & \frac{f_F N_p}{\pi Z_q}\{p(0,x)G(\omega_s, y_0, \omega_p, \gamma)\} \\ & + \{p(1,x)G(\omega_s, y_0(1+\delta), \omega_p, \gamma)\} \\ & + \{p(2,x)G(\omega_s, y_0(1+2\delta), \omega_p, \gamma)\} + \ldots \\ & + \{p(N,x)G(\omega_s, y_0(1+N\delta), \omega_p, \gamma)\}\end{aligned} \tag{4}$$

where G corresponds to $\left[\frac{\omega_s{}^3(\omega_p{}^2 - \gamma^2) - \omega_s\omega_p{}^4}{(\omega_s{}^2 - \omega_p{}^2)^2 + \omega_s{}^2\gamma^2} + i\frac{\omega_s{}^4\gamma}{(\omega_s{}^2 - \omega_p{}^2)^2 + \omega_s{}^2\gamma^2}\right]$ for the inclusion of polydispersity in the Kelvin–Voigt model (eqn (1)) and to $\left[i\omega_s m_p \frac{1}{1 - \frac{\omega_s{}^2}{\omega_p{}^2} + \frac{i\omega}{\gamma}}\right]$ for inclusion in the Maxwell model (eqn (2)). In order to account for polydispersity in the inertial mass, spring constant or drag coefficient, y_0 is chosen to be equal to either m_p, k or ξ, respectively, after which eqn (4) can be used for fitting that accounts for polydispersities in either of the three above parameters m_p, k or ξ.

Experimental

Bacterial strains, culture conditions and harvesting

Streptococcus salivarius HB7 and HBC12 were used in this study. Both *S. salivarius* strains are hydrophilic, and negatively charged, but the two strains differ in their possession of fibrillar surface appendages used to tether themselves to a substratum surface. *S. salivarius* HB7 possesses well-characterized 91 nm fibrils and *S. salivarius* HBC12 is devoid of surface appendages with a demonstrable length.[27] *S. salivarius* strains were pre-cultured in 10 mL of Todd Hewitt Broth (THB, OXOID, Basingstoke, UK) under static conditions, and grown for 24 h at 37 °C. After 24 h, pre-cultures were inoculated into 200 mL of THB and maintained under the above-mentioned conditions for another 16 h. Bacteria were harvested by centrifugation at 5000*g* for 5 min at 10 °C and subsequently washed in 100 mL adhesion buffer (50 mM potassium chloride, 2 mM potassium phosphate, 1 mM calcium chloride, pH 6.8). Next, bacteria were sonicated on ice 3 times for 10 s at 30 W (Vibra Cell Model 375; Sonics and Materials Inc., Danbury, CT) to maximize the number of single bacteria in suspension. Importantly for QCM-D experiments, bacteria were washed once more after sonication to remove any free molecules that might have been released during sonication to prevent molecular mass adsorption to the crystal sensor during bacterial adhesion. Finally, bacteria were diluted to a concentration of 3×10^8 bacteria per mL, as determined by counting in a Bürker–Türk chamber.

Abiotic particles

Polystyrene particles (Bang Laboratories Inc. Fishers, IN, US), with a diameter of 1 μm similar to streptococci, were employed in this study in order to compare abiotic adhesion *versus* biotic particle adhesion. Prior to experiments, particles were washed twice by centrifugation in 10 mL ultrapure water, and diluted to a concentration of 2×10^8 particles per mL in 50 mM KCl.

Preparation of QCM-D sensor surfaces

14 mm-diameter gold-coated quartz sensor crystals (Qsense, Gothenburg, Sweden) were cleaned prior to each experiment by immersion in a 3 : 1 : 1 mixture of ultrapure water (specific resistance >18 MΩ cm), ammonia (NH_3) (Merck, Darmstadt, Germany) and hydrogen peroxide (H_2O_2) (Merck, Darmstadt, Germany) at 70 °C for 15 min, followed by 15 min of UV/Ozone treatment. For QCM-D experiments, gold-coated sensor crystals were left for 24 h in a well-plate.

For coating the QCM-D crystal sensors with a hydrophobic self-assembled monolayer (SAM), the crystals were left immersed in 0.001 M of 1-octadecanethiol dissolved in 100% ethanol for 18 h under mild shaking to obtain a homogenous coating.

To obtain hydrophilic crystal sensors, crystals were immersed in 0.0001 M of 11-mercapto-1-undecanol (Sigma-Aldrich, Zwijndrecht, The Netherlands) in 100% ethanol under the above conditions.

Contact angle measurements

Contact angles were measured on differently coated crystal surfaces with three liquids possessing different polarities (water, formamide, and methyleneiodide), using a homemade goniometer. The contact angles were recorded using a fixed camera for about 5 s after placing a 0.5 μL liquid droplet on a crystal surface. Three droplets of each liquid were randomly placed over one crystal surface, employing three different crystals for each measurement. The droplet contours were detected by grey-value thresholding and contact angles were calculated from the digitized contours using home-made software. Contact angles on each surface were converted to a Lifshitz–van der Waals (γ^{LW}) and acid–base (γ^{AB}) surface free energy component, while the acid–base components were split up into an electron-donating parameter (γ^-) and an electron-accepting (γ^+) parameter[28] according to

$$\begin{bmatrix} \sqrt{\gamma^{LW}_{water}} & \sqrt{\gamma^{+}_{water}} & \sqrt{\gamma^{-}_{water}} \\ \sqrt{\gamma^{LW}_{formamide}} & \sqrt{\gamma^{+}_{formamide}} & \sqrt{\gamma^{-}_{formamide}} \\ \sqrt{\gamma^{LW}_{methyleneiodide}} & \sqrt{\gamma^{+}_{methyleneiodide}} & \sqrt{\gamma^{-}_{methyleneiodide}} \end{bmatrix} \begin{bmatrix} \sqrt{\gamma^{LW}} \\ \sqrt{\gamma^{-}} \\ \sqrt{\gamma^{+}} \end{bmatrix} = \begin{bmatrix} (1+\cos\theta_{water})\cdot\frac{\gamma_{water}}{2} \\ (1+\cos\theta_{formamide})\cdot\frac{\gamma_{formamide}}{2} \\ (1+\cos\theta_{methyleneiodide})\cdot\frac{\gamma_{methyleneiodide}}{2} \end{bmatrix} \quad (5)$$

where γ^{LW} is the Lifshitz–van der Waals surface free energy component and γ^- and γ^+ are the electron-donating and electron-accepting surface free energy parameters, respectively, of the three liquids applied or the solid surface considered (see subscripts). The total surface free energy is denoted as γ, while θ represents the contact angles.

Surface roughness measurements by atomic force microscopy (AFM)

The surface roughnesses of the QCM-D crystal sensors, without coating and with hydrophobic or hydrophilic SAMs, were measured by AFM in contact mode using a silicon nitride cantilever tip (DNP from Bruker, Woodbury, NY, USA). Each crystal sensor was imaged at three randomly chosen locations on the crystal surface and surface plots were generated in order to obtain a three-dimensional perspective of the surface, from which the surface roughness (R_a) was calculated (see Table 1).

QCM-D

All QCM-D experiments were carried out at room temperature using a window-equipped chamber (E1, Qsense, Gothenburg, Sweden). The window chamber containing the sensor crystal was mounted underneath a microscope (Leica DM2500 M, Rijswijk, The Netherlands) equipped with a CCD camera (Model A101, Basler vision technologies, Ahrensburg, Germany), enabling real-time monitoring of particulate adhesion on the QCM-D sensor surface. Frequency and dissipation shifts at 7 different sensor frequencies (5, 15, 25, 35, 45, 55 and 65 MHz) were acquired. Prior to particulate adhesion in the QCM-D, buffer was perfused through the chamber at a flow rate of 300 μL min^{-1} until a steady base line (variations in Δf less than 2 Hz over 5–10 min) was obtained.

Following this, a particulate suspension was perfused through the chamber at a flow rate of 300 μL min^{-1} for 1 h. Subsequently, buffer was perfused again to remove the particulate suspension from the QCM-D chamber, followed by the determination of the number of adhering particles per unit area.

Table 1 Water contact angles, surface free energy components and parameters together with surface roughnesses of QCM-D crystal surfaces with a hydrophobic or hydrophilic SAM-coating. Data represent averages with standard deviations over three droplets on three different crystals

	Crystal with hydrophobic SAM	Gold-coated crystal	Crystal with hydrophilic SAM
Contact angles (degrees)			
Water	90 ± 7	54 ± 3	17 ± 5
Formamide	27 ± 7	17 ± 1	0 ± 0
Methyleneiodide	48 ± 10	37 ± 4	38 ± 8
Surface free energy components and parameters (10^{-3} J m^{-2})			
γ	35 ± 6	55 ± 2	58 ± 0
γ^{LW}	35 ± 6	41 ± 2	40 ± 4
γ^{AB}	0 ± 0	13 ± 0	17 ± 7
γ^-	0 ± 0	15 ± 2	49 ± 3
γ^+	11 ± 5	3 ± 1	2 ± 1
γ^-/γ^+	0 ± 0	5 ± 2	25 ± 2
Surface roughness by AFM (nm)			
R_a	3.0 ± 0.4	3.4 ± 0.3	1.7 ± 0.1

Data analysis

The frequency and dissipation shifts were retrieved from the QCM-D, as illustrated in Fig. 2, and converted into Δf and $\Delta\Gamma$, with $\Delta\Gamma = \Delta D \times f_s/2$. These values were then used to fit the data non-linearly to eqn (1) (Kelvin–Voigt model) or eqn (2) (Maxwell model), using a brute-force, iterative algorithm, written in Python, to obtain parameter values for the spring constant (k), dashpot (ξ), mass of the particle (m_p), and the root mean square deviation (RMSD) of the resulting fit *vis-à-vis* the measured data.[25] Data presented are those yielding the lowest RMSD. A similar iterative algorithm was also used to solve eqn (4) as the extended form of eqn (1) and (2) accounting for a polydispersity index λ for the inertial mass, spring constant and drag force (eqn (3) and (4)) setting λ to 0 (no polydispersity), 2, 5 or 7 (high polydispersity). The polydispersity indices presented are those yielding the lowest RMSD.

Results

The hydrophobicities of the QCM-D crystal surfaces were varied by the application of a hydrophobic and hydrophilic SAM,

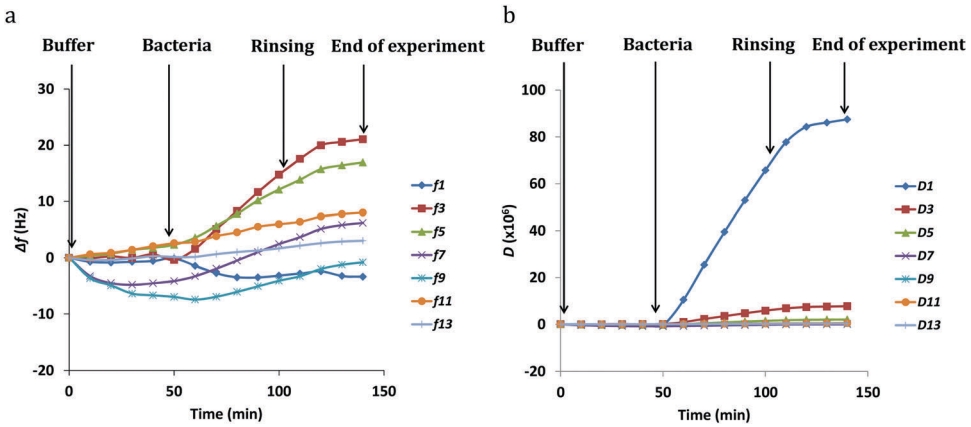

Fig. 2 Example of the changes in frequency (a), and dissipation (b) as a function of time during adhesion of *S. salivarius* HB7 on hydrophobic SAM. *f*1 to *f*13 (a panel) and *D*1 to *D*13 (b panel) correspond to different overtone frequencies (indicated by subscripts in the legends), ranging from 5 to 65 MHz. Note data points may be overlapping.

yielding a wide variation in the water contact angle ranging from 17 to 90 degrees, including the gold-coated crystal with a water contact angle of 54 degrees (see Table 1). Water contact angles are not sufficient to characterize surface hydrophobicity, however, since hydrophobicity is either due to low electron-donating or low electron-accepting surface free energy parameters, as can be calculated from the contact angles with three liquids, as also presented in Table 1. Whereas the Lifshitz–van der Waals surface free energy components of all three surfaces are fairly high, only the hydrophobic SAM-coating demonstrates a zero acid–base surface free energy component. The absence of an acid–base surface free energy component is due to a zero electron-donating and electron-accepting parameter of the hydrophobic SAM, opposite to the gold-coated crystal surface and the hydrophilic SAM, possessing both non-zero electron-donating and electron-accepting surface free energy parameters. Accordingly, the ratio of electron-donating over electron-accepting parameters varies widely across the three surfaces (see also Table 1), indicative of different structuring of water molecules adjacent to the surface.[29] All crystal surfaces employed were extremely smooth in the nanoscale region, although the hydrophilic SAM-layer demonstrated a less rough surface than the hydrophobic one (see also Table 1).

Table 2 presents the number of bacteria and polystyrene particles that adhered to the crystal surfaces after 1 h of perfusing the QCM-D chamber with a particle suspension. The numbers were all on the order of 10^{10} m^{-2}, representing a surface coverage of around 1–10%, sufficiently low to avoid interactions between adhering particles during crystal oscillation. The fibrillated streptococcal strain *S. salivarius* HB7 adhered in similar numbers to all three crystal surfaces ($p > 0.05$; Student's *t*-test). The bald strain, *S. salivarius* HBC12, adhered equally well to the crystal surfaces as did *S. salivarius* HB7, with the exception of the hydrophilic SAM-coated crystal surface to which it adhered in two-fold, significantly ($p < 0.05$, Student's *t*-test) lower numbers than to the gold-coated crystal surface. Polystyrene particles adhered in significantly lower numbers on the hydrophilic SAM-coated crystal compared to the gold-coated crystal

Table 2 The number of adhering streptococci and polystyrene particles per unit area (N_p m^{-2}) on crystal surfaces with different hydrophobicities. Data represent averages with standard deviations over three separate experiments, with separately grown bacterial cultures and differently prepared suspensions

Biocolloids and colloids	Crystal surface	N_p ($\times 10^{10}$ m^{-2})
S. salivarius HB7	Hydrophobic SAM	4.1 ± 0.6
	Gold-coated crystal	3.5 ± 0.4
	Hydrophilic SAM	4.2 ± 1.3
S. salivarius HBC12	Hydrophobic SAM	3.8 ± 1.4
	Gold-coated crystal	3.4 ± 0.4
	Hydrophilic SAM	2.0 ± 0.7
Polystyrene particles	Hydrophobic SAM	1.8 ± 0.7
	Gold-coated crystal	1.0 ± 0.2
	Hydrophilic	2.0 ± 0.3

($p < 0.05$; Student's *t*-test), comparable to the adhesion behavior of the bald streptococcus strain.

An example of the raw QCM-D data as a function of time is presented in Fig. 2 for *S. salivarius* HB7 adhering to a hydrophobic SAM-coated crystal. Frequency as well as dissipation shifts vary over time and with the overtone frequency. Data such as those presented in Fig. 2 and Table 2, were inserted in phenomenological Kelvin–Voigt and Maxwell models, with and without accounting for polydispersity in the forthcoming parts of the Results section.

Fig. 3–5 show examples of the best fits of Kelvin–Voigt and Maxwell parameters for *S. salivarius* HB7, *S. salivarius* HBC12 and polystyrene particles under the experimental conditions specified, respectively, while Tables 3 and 4 summarize the resulting parameters after fitting the QCM-D output for streptococcal and polystyrene particle adhesion to a Kelvin–Voigt or Maxwell model, respectively.

Fits for *S. salivarius* HB7 (Fig. 3) consistently show a frequency of zero crossing (between 5 and 15 MHz) in line with the Dybwad coupled resonator model, whereas *S. salivarius* HBC12 (Fig. 4) and abiotic polystyrene particles (Fig. 5) do not demonstrate frequencies of zero crossing, indicating that the two particles

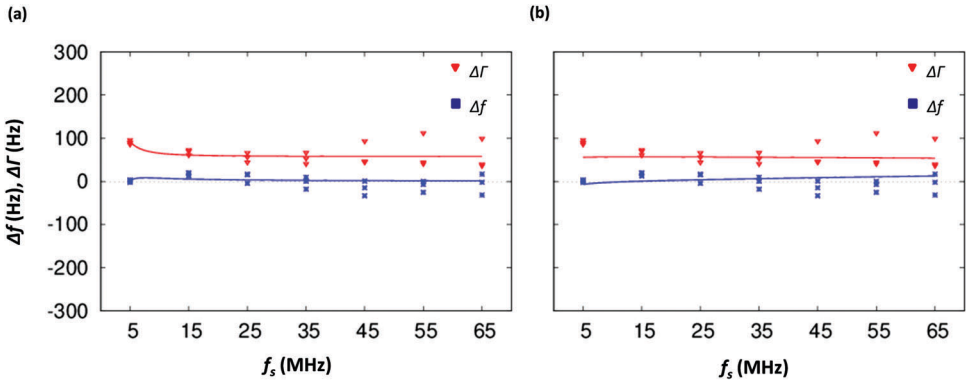

Fig. 3 Examples of the QCM-D responses, Δf and $\Delta\Gamma$ for adhesion of *S. salivarius* HB7 to a hydrophobic SAM-coated crystal surface as a function of the sensor frequency in the absence of a polydispersity index for (a) the Kelvin–Voigt model and (b) the Maxwell model. The raw QCM-D data points that were used for fitting were the end-values of Δf and D (see also Fig. 2) and D was converted to $\Delta\Gamma$.

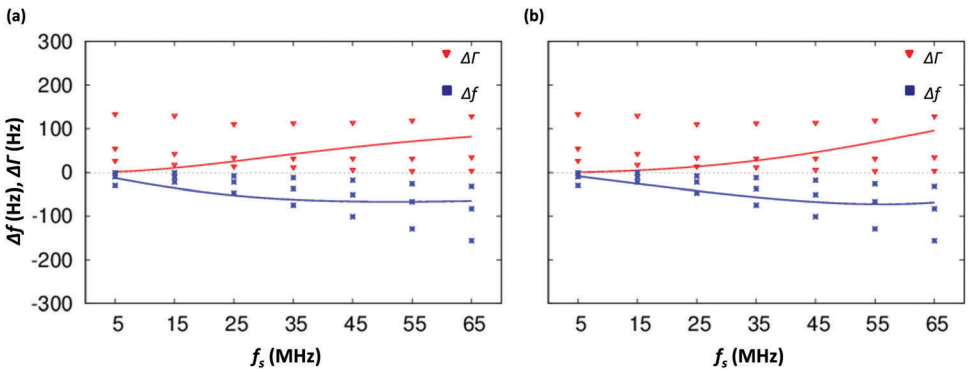

Fig. 4 Examples of the QCM-D responses, Δf and $\Delta\Gamma$ for adhesion of *S. salivarius* HBC12 to a hydrophobic SAM-coated crystal surface as a function of the sensor frequency in the absence of a polydispersity index for (a) the Kelvin–Voigt model and (b) the Maxwell model. The raw QCM-D data points that were used for fitting were the end-values of Δf and D (see also Fig. 2) and D was converted to $\Delta\Gamma$.

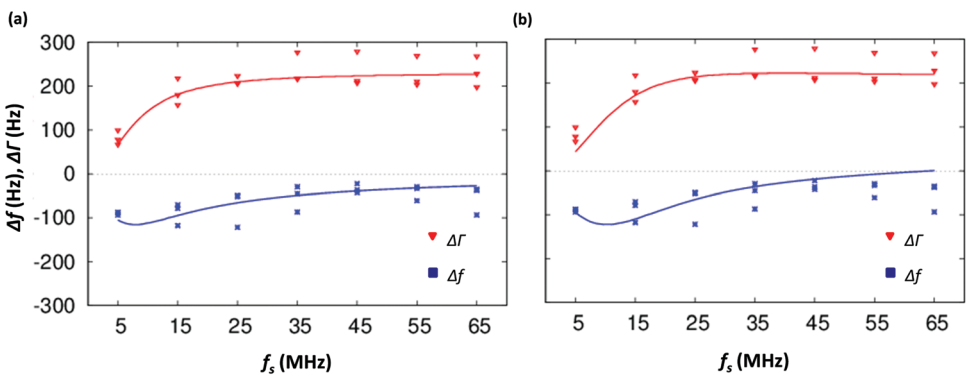

Fig. 5 Examples of the QCM-D responses, Δf and $\Delta\Gamma$ for adhesion of polystyrene to a hydrophobic SAM-coated crystal surface as a function of the sensor frequency for (a) the Kelvin–Voigt model in the absence of a polydispersity index and (b) the Maxwell model in the presence of a polydispersity index (λ employed equals 2) in the spring constant. The raw QCM-D data points that were used for fitting were the end-values of Δf and D (see also Fig. 2) and D was converted to $\Delta\Gamma$.

behave more like an adsorbed mass rather than coupling as a resonator to the QCM-D crystal. The quality of the fits can be judged from the RMSD values in Tables 3 and 4. On average, the RMSD values obtained using the Kelvin–Voigt model (43 ± 13 Hz) are similar to those obtained from the Maxwell model (44 ± 11 Hz). The particle masses obtained for the biotic and abiotic particles range between 1×10^{-16} kg and 12×10^{-16} kg in the Kelvin–Voigt model, whereas in the Maxwell model particle masses between 1×10^{-16} kg and 20×10^{-16} kg are obtained. Therewith all masses obtained are within the same order of magnitude as can be calculated for bacteria (yielding 5×10^{-16} kg) from published bacterial dimensions and densities or

Table 3 Spring constants k, drag coefficients ξ, masses m_p and RMSD values obtained in a Kelvin–Voigt coupled-resonator model, for both the fibrillated (*S. salivarius* HB7) and non-fibrillated (*S. salivarius* HBC12) streptococcal strains as well as for abiotic polystyrene particles. λ indicates the range of polydispersity to obtain the best fit

Bacterial strains	m_p (10^{-16} kg)	k (kg s^{-2})	ξ (10^{-9} kg s^{-1})	λ	RMSD (Hz)
S. salivarius HB7 on hydrophobic SAM	6	0.35	10	0	41
S. salivarius HB7 on gold-coated crystal	6	0.22	9	0	20
S. salivarius HB7 on hydrophilic SAM	5	0.24	5	0	84
S. salivarius HBC12 on hydrophobic SAM	1	0.00	19	0	42
S. salivarius HBC12 on gold-coated crystal	3	0.06	5	0	22
S. salivarius HBC12 on hydrophilic SAM	1	0.45	46	0	22
Polystyrene particles					
On hydrophobic SAM	12	0.00	61	0	39
On gold-coated crystal	5	0.00	113	0	64
On hydrophilic SAM	8	0.00	16	0	55

Table 4 Spring constants k, drag coefficients ξ, masses m_p and RMSD values obtained in a Maxwell coupled-resonator model, for both the fibrillated (*S. salivarius* HB7) and non-fibrillated (*S. salivarius* HBC12) streptococcal strains as well as abiotic polystyrene particles. λ indicates the range of polydispersity to obtain the best fit

Bacterial strains	m_p (10^{-16} kg)	k (kg s^{-2})	ξ (10^{-9} kg s^{-1})	λ	RMSD (Hz)
S. salivarius HB7 on hydrophobic SAM	20	9.75	13	0	48
S. salivarius HB7 on gold-coated crystal	20	15.0	9	0	25
S. salivarius HB7 on hydrophilic SAM	20	2.10	13	0	80
S. salivarius HBC12 on hydrophobic SAM	0	15.0	21	0	44
S. salivarius HBC12 on gold-coated crystal	5	15.0	5	0	23
S. salivarius HBC12 on hydrophilic SAM	1	15.0	45	0	26
Polystyrene particles					
On hydrophobic SAM	10	554	79	2[a]	41
On gold-coated crystal	5	241	141	2[a]	58
On hydrophilic SAM	4	50.2	71	2[a]	51

[a] Indicates polydispersity in k.

calculated from the dimension of the polystyrene particles and their density (yielding 5.5×10^{-16} kg).[30] For *S. salivarius* HBC12, both models yield an identical, small mass of 2×10^{-16} kg on average, while also for polystyrene particles both models yield a similar mass that is comparable with the gravitational mass of polystyrene particles. Interestingly, while both of these particles adhered more in line with mass adsorption theory, particle masses for *S. salivarius* HB7 that adhered more like a coupled resonator differ considerably as obtained from the Kelvin–Voigt (6×10^{-16} kg; see Table 3) *versus* the Maxwell model (20×10^{-16} kg; see Table 4).

Also, the spring constants k obtained from both models differ by orders of magnitude for the three different particle types involved (compare Tables 3 and 4). In the Kelvin–Voigt model, the hydrophobicity of the crystal surface shows no systematic trend with the spring constant obtained, but in the Maxwell model the spring constants of *S. salivarius* HB7 and polystyrene particles were consistently smaller on the hydrophilic crystal surface.

Unlike the spring constants, but similar to the particle masses obtained, both models yielded comparable results for the drag coefficients of mass-adsorbing *S. salivarius* HBC12 and abiotic polystyrene particles. The drag coefficients increased towards to the hydrophilic SAM-coated crystals for the hydrophilic *S. salivarius* HBC12, while oppositely a decrease was observed for the hydrophobic polystyrene particles. For *S. salivarius* HB7 demonstrating coupled resonator characteristics, the drag coefficients obtained are comparable for both models and hardly vary among the different crystal surfaces.

Inclusion of polydispersity in mass, spring constant or drag-force for either bacterial strain did not increase the quality of the fit in Kelvin–Voigt or in Maxwell models. However, for polystyrene particles in the Maxwell model, inclusion of polydispersity in the spring constant yielded a better fit than could be obtained in the absence of polydispersity or including polydispersity in the mass or drag coefficient.

Discussion

Kelvin–Voigt and Maxwell models are both versatile instruments to model and explain the viscoelastic behavior of materials,[4] including biofilms.[6] This study compares the use of coupled resonator approaches based on phenomenological Kelvin–Voigt or Maxwell models and the possible role of polydispersity in the analysis of the QCM-D response to the adhesion of a fibrillated and non-fibrillated streptococcal strain and abiotic polystyrene particles to QCM-D crystal surfaces having different hydrophobicities. The hydrophobicity of a gold-coated QCM-D crystal was varied by application of a hydrophobic or hydrophilic SAM, which differed not only in the water contact angle, but moreover in the ratio between electron-donating and electron-accepting surface free energy parameters. All crystal surfaces were extremely smooth in the nanometer range (Table 1), although the hydrophilic SAM-coating was slightly smoother than the two hydrophobic crystal surfaces. Nevertheless, it is generally considered unlikely that such small nanoscopic differences in R_a will affect bacterial adhesion.[31]

QCM-D responses Δf and $\Delta \Gamma$ to the adhesion of biotic fibrillated streptococci and abiotic polystyrene particles could be fitted equally well using the Kelvin–Voigt or Maxwell model and comparison of RMSD values did not yield an indication as to which model might be preferentially used in the analysis of QCM-D responses from a mathematical perspective. Calculations of bacterial and polystyrene particle masses validated both phenomenological models within wide ranges, but it is uncertain to what extent the QCM-D yields actual gravitational or inertial masses and how the two are related.[17] Chindam *et al.*[4] marked the Kelvin–Voigt model as more accurate than the Maxwell model

based on comparison of the Young's moduli obtained with the real value, but such ''real'' values for the bacterial properties are impossible to obtain. A comparison of the spring constants of bacterial bonds to substratum surfaces with independently obtained literature data is also difficult, not in the least since QCM-D operates at a forced, high frequency in the MHz range, whereas for instance bacterial vibration spectroscopy explores spring constants under natural, Brownian motion induced, low frequency vibrations. Bacterial vibration spectroscopy indicated that the fibrillated streptococcal strain, *S. salivarius* HB7, had higher vibrational amplitudes than its bald mutant strain *S. salivarius* HBC12, corresponding to the spring constants of around 2 and 3×10^{-5} N m^{-1}, respectively,[13] which are 5 orders of magnitude different from those found here. Also spring constants obtained by means of AFM for whole cells, thus not specifically of the bond itself,[32,33] were orders of magnitude different from those obtained here.

Herewith it becomes impossible to conclude which phenomenological model is mathematically or by comparison with other independent methods preferable. Such a conclusion at the same time may be less important than the question of whether the application of either model yields the same or different insights into the physico-chemistry of the bond underlying the phenomenon studied. Both Kelvin–Voigt and Maxwell analyses, bacterial vibration spectroscopy and AFM of the streptococcal bonds point to a stiffer binding of the bald strain *S. salivarius* HBC12 than of the fibrillated *S. salivarius* HB7.[13] In neither of the QCM-D models did inclusion of polydispersity yield a better quality of the fit for streptococcal adhesion. For polystyrene particles only a minor polydispersity (λ equal to 2) in the spring constant was inferred. This suggests that polydispersity plays less of a role in the analysis of QCM-D responses to particle adhesion than proposed before.[17]

In both the Kelvin–Voigt and the Maxwell analyses, the drag coefficient increased for the hydrophilic *S. salivarius* HBC12 on going from the hydrophobic to the hydrophilic crystal surfaces, despite being numerically different in both analyses. These hydrophilic, biotic particles have no or very short surface appendages and concurrently, the QCM-D response suggests that these particles behave on the crystal surface as an adsorbed mass and may thus be more susceptible to the properties of the crystal surface and the resulting water structuring under the influence of the surface, as indicated by the high ratio of electron-donating over electron-accepting parameters, on the hydrophilic SAM-coating. Oppositely for hydrophobic polystyrene particles in both models, the drag coefficient decreases when the ratio of electron-donating over electron-accepting parameters increases, suggesting that hydrophobic particles experience less drag due to structured water on the surface than hydrophilic ones. The fact that the drag coefficient of *S. salivarius* HB7 is quite similar on hydrophilic and hydrophobic crystal surfaces combined with its propensity to bind to the sensor crystal as a coupled resonator suggests that the drag coefficient of resonator coupled particles is much more influenced by the viscosity of the bulk water, *i.e.* far above the crystal surface than by the structured water adjacent to the crystal (note that its fibrils are 91 nm long).

Separating the particle types involved in this study into mass adsorbing and resonator coupling ones reveals an interesting difference between the Kelvin–Voigt model and the Maxwell model. Whereas for *S. salivarius* HBC12 and polystyrene particles, the particle masses derived are nearly the same in both models, *S. salivarius* HB7 has a four-fold higher mass in the Maxwell model than in the Kelvin–Voigt model. Pending the uncertainty regarding the proper mass (gravitational or inertial) derived in QCM-D and its ''real'' value, and the possible impact on the spring constants and the drag coefficients derived, Johannsmann[5] suggested to use the ratio $\frac{\omega\xi}{k}$ or $\tan(\delta)$ as a ''lossiness'' parameter to be derived from QCM-D analyses, which is solely based on the ratio between the drag coefficients and spring constants of the bond.

A summary of the ''lossiness'' values in Table 5 for both models yields the general conclusion that the Maxwell model yields predominantly elastic bond characteristics with minimal damping contributions. This can be explained by the fact that in the Kelvin–Voigt model the spring and the dashpot in parallel aid in concert in particle movement (Fig. 6a), whereas in the Maxwell model the spring and the dashpot act completely independent of each other and the dashpot is not forced to participate in the response to the oscillations of the crystal by the spring (Fig. 6b). Possibly this explains why the Kelvin–Voigt model has been judged to be preferable over the Maxwell model in explaining the thermo-mechanical response of metals under elastic cyclic loading.[4] This may put a larger emphasis on the elastic response in the Maxwell model compared with the Kelvin–Voigt model as suggested by the small ''lossiness'' values for the Maxwell model in Table 5. However, the fact that fluid is present all around the adhering particles and the bond itself is hydrated indicates a necessary damping contribution to the bond, or lossiness, which the Kelvin–Voigt model allows for in contrast to the Maxwell model (see Table 5). This realization may also explain why *S. salivarius* HB7 has a four-fold higher mass in the Maxwell model than in the Kelvin–Voigt model, as the dashpot does not become activated by the spring to make the particle resonate in tune with the crystal through the bulk liquid. However, also two Maxwell elements placed in parallel,

Table 5 Lossiness $\tan(\delta)$ obtained for both the fibrillated (*S. salivarius* HB7) and non-fibrillated (*S. salivarius* HBC12) streptococcal strains as well as for abiotic polystyrene particles in the Kelvin–Voigt and Maxwell models

Bacterial strains	$\tan(\delta)$ Kelvin–Voigt	$\tan(\delta)$ Maxwell
S. salivarius HB7 on hydrophobic SAM	0.14	0.01
S. salivarius HB7 on gold-coated crystal	0.21	0.00
S. salivarius HB7 on hydrophilic SAM	0.11	0.03
S. salivarius HBC12 on hydrophobic SAM	>1	0.01
S. salivarius HBC12 on gold-coated crystal	0.41	0.00
S. salivarius HBC12 on hydrophilic SAM	0.51	0.01
Polystyrene particles		
On hydrophobic SAM	>1	0.00
On gold-coated crystal	>1	0.00
On hydrophilic SAM	>1	0.00

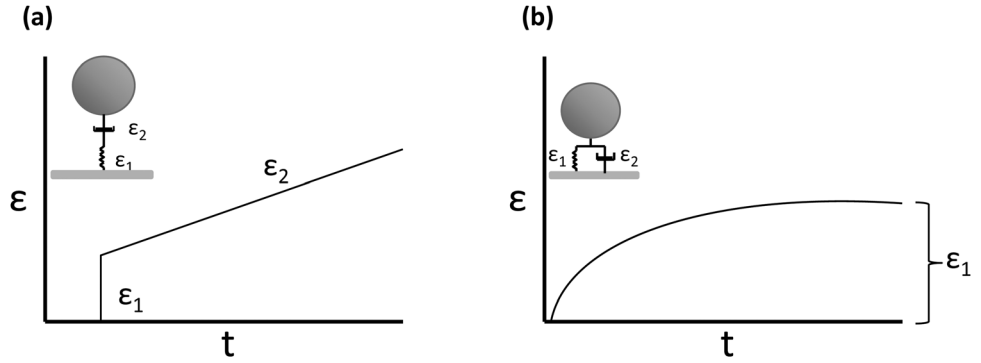

Fig. 6 Schematic presentation of the strain of a bond in the Maxwell (a) *versus* Kelvin–Voigt (b) model as a function of time[8] during application of a constant stress, as experienced by adhering (bio)colloidal particles exposed to fluid shear. (a) The dashpot in parallel with the spring dampens the spring response. The stretching continues to a plateau level. (b) Spring and dashpot in series act independently. The spring immediately stretches to a constant strain, but the dashpot continues to stretch without being limited until ultimately the bond breaks.

as often employed to model the viscoelastic response of biofilms,[6] with one being predominantly elastic and the other mainly viscous would in essence resemble a single Kelvin–Voigt element and give the same response. For biofilms, it appears trivial that their viscoelastic response comprises too many independent processes to be captured in one Kelvin–Voigt or Maxwell element, but it cannot be ruled out that also the QCM-D response to single particle adhesion comprises multiple Maxwell elements that might pairwise resemble a Kelvin–Voigt element. Unfortunately, the use of multiple elements in analogy with the analysis of stress relaxation of biofilms for fitting the QCM-D response of adhering bacteria is mathematically impossible due to the limited number of frequencies that can be observed in QCM-D.

Conclusion

In conclusion, we demonstrated a new method to quantitatively analyze QCM-D responses of (bio)colloid adhesion to hydrophobic and hydrophilic crystal surfaces to obtain viscoelastic bond properties. The use of a phenomenological Kelvin–Voigt or Maxwell model in a coupled-resonator approach yielded good fits to the QCM-D data. Inclusion of polydispersity in the spring constant only improved the quality of the fits in a Maxwell model for hydrophobic polystyrene particles. In the Kelvin–Voigt and Maxwell models, the drag coefficient increased for the bald streptococcus with the ratio of electron-donating over electron-accepting parameters of the crystal surface, likely because it coupled closer to the crystal surface and more like an adsorbed mass than the fibrillated strain. For the fibrillated strain, the drag coefficient was similar on all crystal surfaces. Thus, the drag experienced by resonator-coupled, hydrophilic particles is more influenced by the viscosity of the bulk water than by the structured water adjacent to the crystal surface that is probed by particles coupled without a tether, positioning the particle just above the thin interfacial layer of structured water on a surface.

Kelvin–Voigt and Maxwell models both have their virtues in analyzing the phenomenon of bacterial or particle adhesion when it comes to fitting of coupled resonator models to QCM-D data. Apart from the above conclusions that could be drawn on the basis of both models, the Maxwell model in general emphasized the elastic response more than the Kelvin–Voigt model. Placed in series with a dashpot, the elastic response in the Maxwell model acts independently of damping. In the Kelvin–Voigt model, the spring is placed in parallel with the dashpot and continuously opposed in its response by the dashpot. Exposed to fluid shear, this implies that in a Maxwell model, the bond elongates until rupture, which is unrealistic and may make the Kelvin–Voigt model preferable.

Funding

This study was entirely funded by UMCG, Groningen, The Netherlands.

Conflicts of interest

The authors declare no potential conflicts of interest with respect to authorship and/or publication of this article. HJB is also the director of a consulting company SASA BV. The opinions and assertions contained herein are those of the authors and are not construed as necessarily representing the views of the funding organization or their respective employer(s).

Acknowledgements

We thank Dr Philipp Kühn from the Department of Biomedical Engineering, Groningen, for performing the AFM measurements on QCM-D crystals.

References

1 A. L. J. Olsson, N. Arun, J. S. Kanger, H. J. Busscher, I. E. Ivanov, T. A. Camesano, Y. Chen, D. Johannsmann, H. C. van der Mei and P. K. Sharma, *Soft Matter*, 2012, **8**, 9870.

2 V. Vadillo-Rodriguez, S. R. Schooling and J. R. Dutcher, *J. Bacteriol.*, 2009, **191**, 5518–5525.

3 M. Ramstedt, R. Nakao, S. N. Wai, B. E. Uhlin and J.-F. Boily, *J. Biol. Chem.*, 2011, **286**, 12389–12396.
4 C. Chindam, K. C. Venkata, K. Balasubramaniam and R. V. Prakash, *Mater. Sci. Eng., A*, 2013, **560**, 54–61.
5 D. Johannsmann, *Sens. Bio-Sensing Res.*, 2016, **11**, 86–93.
6 B. W. Peterson, Y. He, Y. Ren, A. Zerdoum, M. R. Libera, P. K. Sharma, A.-J. van Winkelhoff, D. Neut, P. Stoodley, H. C. van der Mei and H. J. Busscher, *FEMS Microbiol. Rev.*, 2015, **39**, 234–245.
7 T. Shaw, M. Winston, C. J. Rupp, I. Klapper and P. Stoodley, *Phys. Rev. Lett.*, 2004, **93**, 098102.
8 W. Flügge, in *Viscoelasticity*, ed. W. Prager and J. Kestin, Blaisdell Publising company, 1967, pp. 3–21.
9 G. Francius, J. Hemmerlé, V. Ball, P. Lavalle, C. Picart, J. C. Voegel, P. Schaaf and B. Senger, *J. Phys. Chem. C*, 2007, **111**, 8299–8306.
10 V. Vadillo-Rodriguez, T. J. Beveridge and J. R. Dutcher, *J. Bacteriol.*, 2008, **190**, 4225–4232.
11 Y. He, B. W. Peterson, M. A. Jongsma, Y. Ren, P. K. Sharma, H. J. Busscher and H. C. van der Mei, *PLoS One*, 2013, **8**, e63750.
12 B. W. Peterson, H. J. Busscher, P. K. Sharma and H. C. van der Mei, *Microsc. Microanal.*, 2014, **20**, 912–915.
13 L. Song, J. Sjollema, P. K. Sharma, H. J. Kaper, H. C. van der Mei and H. J. Busscher, *ACS Nano*, 2014, 8457–8467.
14 T. Dabros, P. Warszynski and T. G. M. van de Ven, *J. Colloid Interface Sci.*, 1994, **162**, 254–256.
15 M. Kamiti and T. G. M. Van De Ven, *Macromolecules*, 1996, **29**, 1191–1194.
16 K. C. Neuman and A. Nagy, *Nat. Methods*, 2008, **5**, 491–505.
17 A. L. J. Olsson, H. C. van der Mei, D. Johannsmann, H. J. Busscher and P. K. Sharma, *Anal. Chem.*, 2012, **84**, 4504–4512.
18 G. Sauerbrey, *Z. Phys.*, 1959, **155**, 206–222.
19 G. L. Dybwad, *J. Appl. Phys.*, 1985, **58**, 2789–2790.
20 D. Johannsmann, *Macromol. Chem. Phys.*, 1999, **516**, 501–516.
21 A. Pomorska, D. Shchukin, R. Hammond, M. A. Cooper, G. Grundmeier and D. Johannsmann, *Anal. Chem.*, 2010, **82**, 2237–2242.
22 D. Johannsmann, *Phys. Chem. Chem. Phys.*, 2008, **10**, 4516–4534.
23 J. N. D'Amour, J. J. R. Stålgren, K. K. Kanazawa, C. W. Frank, M. Rodahl and D. Johannsmann, *Phys. Rev. Lett.*, 2006, **96**, 058301.
24 F. A. Firestone and B. F. A. Firestong, *J. Acoust. Soc. Am.*, 1933, **4**, 249.
25 R. van der Westen, H. C. van der Mei, H. De Raedt, A. L. J. Olsson, H. J. Busscher and P. K. Sharma, *Colloids Surf., B*, 2016, **148**, 255–262.
26 M. Evans, N. Hastings and B. Peacock, *Statistical Distributions*, 2000, vol. 2.
27 H. C. van der Mei, A. J. Leonard, A. H. Weerkamp, P. G. Rouxhet and H. J. Busscher, *J. Bacteriol.*, 1988, **170**, 2462–2466.
28 C. Logofatu, C. C. Negrila, R. V. Ghita, F. Ungureanu, C. Cotirlan, A. S. Manea, M. F. Lazarescu and C. Ghica, *Cryst. Silicon: Prop. Uses*, 2011, **1**, 2–42.
29 C. J. van Oss and R. F. Giese, *J. Dispersion Sci. Technol.*, 2004, **25**, 631–655.
30 M. Godin, A. K. Bryan, T. P. Burg, K. Babcock and S. R. Manalis, *Appl. Phys. Lett.*, 2007, **91**, 123121.
31 V. K. Truong, R. Lapovok, Y. S. Estrin, S. Rundell, J. Y. Wang, C. J. Fluke, R. J. Crawford and E. P. Ivanova, *Biomaterials*, 2010, **31**, 3674–3683.
32 A. Méndez-Vilas, A. M. Gallardo-Moreno and M. L. González-Martín, *Microsc. Microanal.*, 2007, **13**, 55–64.
33 X. Yao, J. Walter, S. Burke, S. Stewart, M. H. Jericho, D. Pink, R. Hunter and T. J. Beveridge, *Colloids Surf., B*, 2002, **23**, 213–230.